Location and function of vesicle clusters, active zones and Ca^{2+} channels in the lamprey presynaptic terminal

Huzefa Photowala, Rachel Freed and Simon Alford

Department of Biological Sciences, University of Illinois at Chicago, 840 West Taylor Street, Chicago, IL 60607, USA

Synaptic transmission requires spatial and temporal coordination of a specific sequence of events. The trigger for synaptic vesicle exocytosis is Ca^{2+} entry into presynaptic terminals, leading to neurotransmitter release at highly specialized sites known as active zones. Ca^{2+} channel proximity to exocytotic proteins and vesicle clusters at active zones have been inferred from biochemical, histological and ultrastructural data, but direct evidence about functional relationships between these elements in central synapses is absent. We have utilized the lamprey giant reticulospinal synapse to characterize functional colocalization of known synaptic markers in the presynaptic terminal, as well as their reliability during repeated activation. Recycling vesicle clusters, surrounding actin filaments, and physiologically relevant Ca^{2+} influx all show identical morphological distribution. Ca^{2+} influx is mediated by clusters of Ca^{2+} channels that colocalize with the vesicle clusters, defined by imaged sites of vesicle recycling and actin localization. Synaptic transmission is inhibited by block of actin depolymerization, but Ca^{2+} signalling is unaffected. Functional Ca^{2+} channels are localized to presynaptic clusters, and Ca^{2+} transients at these sites account for neurotransmitter release based on their spatial and temporal profiles. Ca^{2+} transients evoked by single axonal action potentials are mediated solely by voltage-operated Ca^{2+} channel activation, and slower Ca^{2+} rises observed throughout the axon result from Ca^{2+} diffusion from the synaptic regions. We conclude that at lamprey giant reticulospinal synapses, Ca^{2+} channels and release sites colocalize, creating a close spatial relationship between active zones and Ca^{2+} entry sites, which is necessary for site-specific, Ca^{2+}-dependent secretion.

(Resubmitted 24 May 2005; accepted after revision 30 August 2005; first published online 1 September 2005)
Corresponding author S. Alford: Department of Biological Sciences, University of Illinois at Chicago, 840 W. Taylor Street, Chicago, IL 60607, USA. Email: sta@uic.edu

Synaptic transmission requires very close temporal coordination of a specific sequence of events to transmit information from the presynaptic terminal to its postsynaptic target. The trigger for neurotransmitter release is Ca^{2+} entry to the presynaptic terminal and, consequently, the relative locations of ion channels, vesicles, core complex and associated protein machinery of the release apparatus are critical to the function of the presynaptic terminal. These components have been subject to intense scrutiny, sufficient to generate a rudimentary understanding of the importance of the structural elements of the terminal in its function (Rosenmund *et al.* 2003; Zhai & Bellen, 2004).

Synaptic vesicles are clustered at release sites, and physiological evidence has lead to the hypothesis that they are located extremely close to presynaptic Ca^{2+} channels that initiate vesicle fusion and the subsequent release of neurotransmitter (Augustine *et al.* 1991). Electron microscope tomography from presynaptic terminals has further demonstrated the spatial arrangement and associations of structural components at release sites (Harlow *et al.* 2001; Gustafsson *et al.* 2002). Active zone architecture helps to dock the vesicles and anchor the channels, and this provides both a particular spatial relationship and a structural linkage between these components of exocytosis.

In particular, presynaptic Ca^{2+} channels are believed to colocalize with the release machinery that controls synaptic vesicle fusion (Catterall, 1999; Spafford & Zamponi, 2003). This was first apparent from experiments to determine Ca^{2+} diffusion times during action-potential-evoked release in the squid giant synapse (Adler *et al.* 1991; Llinas *et al.* 1992; Smith *et al.* 1993). Similar experiments at other synapses have demonstrated essentially the same results, albeit with some variability (Haydon *et al.* 1994; Heidelberger *et al.* 1994; Schneggenburger & Neher, 2000). It has become apparent that Ca^{2+} channels are held in a close physical

 DOI: 10.1113/jphysiol.2005.091314

relationship with the target Ca^{2+}-binding protein, even if the identity of that protein has not yet been unequivocally accepted (Zamponi, 2003).

Histochemical and biochemical assays have demonstrated much of the physical relationship between Ca^{2+} channels and the presynaptic targets of Ca^{2+} (Walrond & Reese, 1985; Robitaille *et al.* 1990; Zhang *et al.* 2000; Kawasaki *et al.* 2004; Sidi *et al.* 2004). The effect of the geometrical relationship among synaptic vesicles, the Ca^{2+} channel, and the proteins of the release machinery on neurotransmitter release has also been inferred from modelling studies (Cooper *et al.* 1996; Shahrezaei & Delaney, 2004). However, what is less clear is the functional relationship between Ca^{2+} channels and the release apparatus at any given synapse. At any time, Ca^{2+} channel function is subject to a number of possible modifying effects; these include the phosphorylation state of the channel (Hell *et al.* 1994; Tareilus & Breer, 1995), whether it is subject to modification by G proteins through the action of $G\beta\gamma$ (Ikeda, 1996; Zamponi, 2001; Dolphin, 2003*b*), and what βCa^{2+} channel subunit is present, if any, at the membrane inserted channel (Dolphin, 2003*a*; Richards *et al.* 2004).

Indeed, it is apparent that elements of the presynaptic terminal must be in close physical contact in order to function. However, there remains little information on the reliability of these relationships from stimulus to stimulus at any given presynaptic terminal (Zenisek *et al.* 2003). For example, we know little of the reliability of Ca^{2+} entry at any given synaptic entry site, nor do we know whether all synapses show functional Ca^{2+} channel activity at all times, or whether functional Ca^{2+} channel activity is isolated to release sites or is distributed more widely in presynaptic terminals.

We have set out to address this issue by determining the functional colocalization of known synaptic markers in the lamprey giant axon, and the stimulus-to-stimulus reliability of their response. The ability to record directly from these giant synapses, and the accessibility to the intracellular milieu of the presynaptic compartment, have enabled use of this terminal in investigations of other presynaptic proteins and their role in neuronal function (Pieribone *et al.* 1995; Shupliakov *et al.* 1997; Morgan *et al.* 2004). We have chosen to relate three key markers of synaptic physiology whose anatomical relationships at presynaptic terminals are inferred from extensive investigation at the electron microscope level (Gustafsson *et al.* 2002; Bloom *et al.* 2003), but which are less well physiologically defined. These components are action-potential-driven Ca^{2+} transients, synaptic vesicle clusters and actin filaments known to localize around vesicle clusters. Injection of the toxin phalloidin, which prevents actin polymerization, clearly marked synapses and blocked synaptic transmission over long time courses, but had no measurable effect on Ca^{2+} entry. Furthermore, Ca^{2+} channel activation, and consequent Ca^{2+} entry, were found to be reliable from stimulus to stimulus, and highly localized to the presynaptic specialized regions on the axons. Ca^{2+} transients recorded in axons demonstrated rapid rising and decaying responses at the presynaptic terminals and a later sustained Ca^{2+} rise resulting from diffusion throughout the axon. This transient is readily explained by the action potential activation of voltage-gated Ca^{2+} channels clustered at 'hotspots' on the axon plasma membrane, colocalized with synaptic release zones. In contrast, release of Ca^{2+} from internal stores did not contribute to the Ca^{2+} signal following single axonal action potentials.

Methods

Experiments were performed on the isolated spinal cords of larval lampreys (*Petromyzon marinus*). The animals were anaesthetized with tricaine methanesulphonate (MS-222; 100 mg l^{-1}; Sigma, St Louis, MO, USA), decapitated, and dissected in a cold saline solution (Ringer) of the following composition (mM): 100 NaCl, 2.1 KCl, 2.6 $CaCl_2$, 1.8 $MgCl_2$, 4 glucose, 5 Hepes, adjusted to a pH of 7.60. Procedures conformed to institutional guidelines (University of Illinois at Chicago, Animal Care Committee).

Electrophysiology

Axons were recorded with conventional sharp microelectrodes containing 1–3 M KCl. For those experiments in which phalloidin was injected into the presynaptic terminal, the phalloidin (labelled with Alexa 568; Molecular Probes, Eugene, OR, USA) was previously dissolved in deionized water at a concentration of 3 units μl^{-1} (final concentration 100 μM) and stored at -20°C for no longer than 4 weeks. Prior to the experiment, this stock solution was added to an equal volume of 3 M KCl, and the electrode was filled with this combination. Electrode impedances ranged from 20 to 50 MΩ. Phalloidin was applied to the interior of the recorded axon by pressure ejection from the microelectrode (Fig. 1*A*).

Patch electrodes for whole-cell pre- and postsynaptic recordings contained (mM): 102.5 caesium methane sulphonate, 1 NaCl, 1 $MgCl_2$, 5 EGTA, 5 Hepes, pH adjusted to 7.2 with CsOH. Patch electrodes for cell-attached recordings of Na^+ or K^+ channels contained Ringer plus 4-aminopyridine (4-AP; 1 mM) to block K^+ currents and allow recordings of Na^+ currents, or TTX (1 μM) to block Na^+ currents and allow recordings of K^+ currents. To attempt to record Ca^{2+} channels, the electrodes contained 1 mM 4-AP and 1 μM TTX, and between 2.6 and 100 mM $BaCl_2$. Osmolarity and pH were

adjusted to physiological levels (270 mosmol l^{-1} and 7.6, respectively).

Imaging

Confocal imaging was performed using a modified Biorad MRC 600 confocal microscope. Two excitation wavelengths were used (488 nm argon ion and 568 nm krypton–argon) through an AOTF-coupled fibre optic launch (Prairie Technologies, Madison, WI, USA). Excitation was applied through a custom dichroic mirror with sharp excitation bands matching the two laser wavelengths (Omega Optical). Two detectors were placed after a second dichroic, with a transmission band from 500 to 560 nm and long pass reflection from 580 nm. Emission filters were band pass (500–560 nm) and long pass (above 580 nm). The photomultiplier outputs were amplified with low-noise current amplifiers (Stanford Instruments, CA, USA) and digitized to 12 bits with a National Instruments board and custom software written under Matlab (Mathworks). The scan head mirrors were driven though the MRC 600 scan head amplifiers with the same custom software. This software is available on our website (http://alford.bios.uic.edu).

CCD imaging was performed on an Olympus BXW 50 microscope equipped with a Hammamatsu ORCA camera. Excitation was by a Sutter Instruments DG4 with band pass excitation (475–505 and 560–570 nm) and band pass emission (510–550 and 580–700 nm).

Application of FM dye

FM2-10 (100 μM) was applied as a stream from a small pipette placed over the surface of the spinal cord (Fig. 1*A*). Constant flow was ensured by a syringe pump. Two thousand stimuli were applied to a microelectrode recorded axon during the dye application, while the presence of the dye in the tissue surrounding the axons was confirmed by imaging. Dye application was subsequently terminated. During this staining protocol, postsynaptic activity was blocked with glutamate receptor antagonists 6-cyano-7-nitroquinoxaline-2,3-dione (CNQX) and D-aminophosponovalerate (AP5) (5 and 100 μM, respectively). Excess dye was removed with Advasep 7 (Kay *et al.* 1999; 1 mM, 1 min; Cydex, Inc., Lenexa, KS, USA) to reveal areas of stimuli-dependent staining.

Retrograde labelling of reticulospinal axons with Ca^{2+}-sensitive dye

Reticulospinal axons were filled with Ca^{2+}-sensitive dye by 16–22 h applications of dextran–amine conjugates of Ca^{2+}-sensitive dyes, Oregon Green 488 BAPTA-1 or Fluo-4

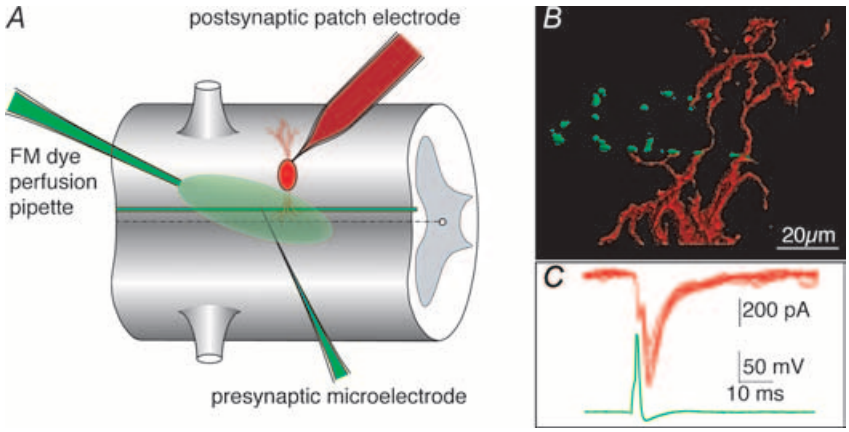

Figure 1. Phalloidin puncta on presynaptic axons are apposed to dendrites of postsynaptic cells at the lamprey giant synapse
A, model of the recording arrangements. Presynaptic axons were recorded with sharp microelectrodes through which microinjections (e.g. phalloidin) were made. In paired-cell recordings, postsynaptic neurones were recorded under whole-cell patch-clamp conditions. FM dyes were applied as a continuous stream over the ventral surface of the spinal cord while the recorded axon was stimulated through the presynaptic microelectrode. *B*, the lamprey giant axon, labelled with phalloidin (Alexa Fluor 488; green) injected through a microelectrode to mark actin surrounding vesicle clusters. The axon makes *en passant* synapses with ventral horn neurones (red) simultaneously recorded with a patch pipette filled with red fluorescent dye (Alexa Fluor 568). *C*, synaptic responses (red) evoked by action potentials (green) in the presynaptic axon. Recordings were from the imaged pair taken simultaneously to the confocal image stacks shown.

dextran (McClellan *et al.* 1994; Molecular Probes). Dye (5 mM) was applied by the internal perfusion of a glass pipette into which the cut end of the spinal cord was drawn by suction. The perfusion apparatus consisted of a 10 μl syringe (Hamilton, Reno, NV, USA) attached by thin tubing to one of two ports of a patch pipette holder, which in turn was connected to a short segment of silica tubing drawn to a thin tip and inserted within 50 μm of the distal tip of the glass pipette. Because dextran-conjugated dyes are only taken up into recently cut axons, the dye was injected into the pipette within 1 min of the cord being cut.

Calibration of the Ca^{2+}-sensitive dyes

The dye sensitivity to Ca^{2+} was determined using the same optical path (confocal microscope) that was used to measure Ca^{2+} transients in the tissue. Dyes (5 μM) were prepared in blends of two Ca^{2+} buffer standards: 10 mM K_2EGTA, 100 mM KCl and 30 mM Mops; and 10 mM CaEGTA 100 mM KCl and 30 mM Mops; both at pH 7.2 (Molecular Probes), to make an 11-point standard curve. The dye/buffer mix was placed between coverslips cooled from below with a liquid cooling system to 10°C, and imaged from above with the ×40 water immersion lens over the upper coverslip.

Imaging two dyes

FM2-10 has a broad emission band, such that fluorescence is seen in both short wavelength (band pass) and long wavelength (long pass) detectors in our recording arrangement. Consequently, to obtain signal separation between FM2-10 and the colocalized Alexa-568-labelled phalloidin, the dyes were not simultaneously imaged. FM and fluorescence were detected by excitation with the 488 nm line and band pass detection (500–560 nm): an arrangement that detected adequate FM2-10 emission but no phalloidin. Alexa-568-labelled phalloidin fluorescence could then be separately detected by switching to the 568 nm laser for excitation and long pass detection (greater than 580 nm): an arrangement that detected excellent phalloidin Alexa 568 fluorescence but no FM dye. Phalloidin and the Ca^{2+}-sensitive dye Oregon Green 488 were readily detected simultaneously on the two photomultiplier channels using simultaneous excitation with both laser lines.

Results

Phalloidin puncta are apposed to postsynaptic dendrites

Reticulospinal axons of the lamprey spinal cord show numerous *en passant* synaptic connections at all segmental levels in the lamprey spinal cord (Rovainen, 1974), such that motoneuronal and interneuronal dendrites surround the axons (Cochilla & Alford, 1999). To demonstrate the location of synaptic contacts on the presynaptic axons, we made paired-cell recordings to label and image reticulospinal axons and their postsynaptic target neurones (Fig. 1*A* and *B*). Paired recordings were made by whole-cell patch clamping ventral horn neurones, and subsequently recording from giant axons with a microelectrode. Pairs were identified electrophysiologically by evoking a presynaptic action potential (Fig. 1*C*). In the postsynaptic neurone, this evoked a compound excitatory postsynaptic current (EPSC) composed of an electrical EPSC with an invariant amplitude and delay from the presynaptic action potential, followed by variable amplitude chemical EPSC that has previously been shown to be glutamatergic (Buchanan *et al.* 1987; Brodin *et al.* 1988). For imaging purposes, fluorescence-labelled phalloidin (Alexa 488 phalloidin; Molecular Probes) was included in the presynaptic microelectrode solution, and dextran-conjugated Alexa Fluor 568 was included in the postsynaptic patch solution. After stable EPSCs had been recorded, the axon was pressure injected with the fluorescently labelled phalloidin. Alexa Fluor freely diffused from the patch solution into the postsynaptic ventral horn neurone. The preparation was imaged by confocal microscopy of the live preparation during the course of the electrophysiological recording from both neurones. Data were reconstructed offline. Phalloidin binds to and stabilizes actin filaments and has been shown to label synaptic structures at this terminal (Shupliakov *et al.* 2002). We demonstrate later in the manuscript that these puncta colocalize in all cases with clusters of recycling vesicles. The punctate distribution of phalloidin staining (Fig. 1*B*, green) indicates the numerous active zones along the axons. Dendrites and spines of the postsynaptic cell make contact with these phalloidin puncta. Using this close apposition as a criteria for synaptic contacts, and based on the labelling of synapses with phalloidin at the electron microscopic level (Shupliakov *et al.* 2002), in three synapses examined in this way, reticulospinal axons made between 5 and 12 estimated synaptic contacts with one postsynaptic target neurone.

Phalloidin puncta colocalize with sites of evoked Ca^{2+} entry

We wished to determine whether physiologically activated Ca^{2+} transients evoked in giant reticulospinal axons correspond to anatomical correlates of presynaptic structures in these axons. We demonstrated above that actin labelled with presynaptic injection of phalloidin forms appositions with synaptically coupled neurone pairs. Others have previously demonstrated that actin

surrounds presynaptic vesicle clusters and synaptic active zones in the lamprey reticulospinal axons (Pieribone *et al.* 1995; Bloom *et al.* 2003). If Ca^{2+} transients evoked by presynaptic action potentials localize only to these synaptic zones, then Ca^{2+} hotspots should colocalize with phalloidin labelling subsequently applied to the axon, while conversely, Ca^{2+} responses will be seen at points previously identified by phalloidin labelling. To investigate this, we used a spectrally separable Ca^{2+} indicator and fluorescently tagged phalloidin in the same giant axon.

We recorded the action-potential-evoked Ca^{2+} responses using the high-affinity Ca^{2+}-sensitive dye, Oregon Green 488 BAPTA-1 (Molecular Probes) in the reticulospinal axons. Axons were retrogradely labelled with the dye, and subsequently recorded from with a microelectrode filled with phalloidin tagged to Alexa Fluor 568. The axons were stimulated through the microelectrode with a 2 ms depolarizing pulse to evoke a single action potential (Fig. 2*Aa*). Presynaptic Ca^{2+} entry sites were identified by scanning along the plasmalemma of the axons while stimulating with the microelectrode. To detect the fast change in the presynaptic $[Ca^{2+}]_i$, images were collected at high speed by scanning a laser at 2 ms intervals over a single line positioned at the axonal plasmalemma (see Methods, and Fig. 6 for more detail). Upon action potential invasion of the terminal, Ca^{2+} entry occurred at localized and discrete 'hotspots' along the length of the axon (Fig. 2*A*). Following identification of the Ca^{2+} hotspots, the axon was pressure injected with fluorescently labelled phalloidin (Alexa Fluor 568 phallodin; Molecular Probes) to mark the active zones in the axon. In a total of six preparations, all of the Ca^{2+} hotspots identified prior to injection of phalloidin ($n = 9$) showed a phalloidin punctum at the same location (Fig. 2*Ab*).

Phalloidin additionally labelled a large number of puncta in the same axon. These puncta were at sites where Ca^{2+} hotspots were not seen because the line scanning technique, necessary to resolve the rapidly rising and decaying Ca^{2+} signal, samples only a one-dimensional line on the three-dimensional axon surface. These newly resolved phalloidin puncta were therefore investigated to determine whether Ca^{2+} signals were evoked with action potentials. Line scanning was performed with the 488 nm excitation laser through the site of phalloidin hotspots. Every such identified phalloidin punctum demonstrated a resolvable Ca^{2+} signal (18 puncta in 8 axons; Fig. 2*Ac* and *B*).

We can conclude that all points in axons with identifiable action-potential-evoked Ca^{2+} transients also show actin clusters, and, conversely, all actin clusters show action-potential-evoked Ca^{2+} hotspots. It is also clear that phalloidin did not prevent Ca^{2+} entry evoked by single action potentials in the giant axons. Presynaptic Ca^{2+} transients were recorded up to 30 min following the presynaptic injection of phalloidin.

Recycling vesicle clusters are located at active zones

Synaptic vesicle cycling at presynaptic terminals can be visualized with styryl dyes (Betz & Bewick, 1992). We sought to determine whether synaptic vesicle clusters colocalize with phalloidin and Ca^{2+} transients. Synaptic vesicle clusters in individual giant axons were labelled with the styryl dye FM2-10. A single presynaptic axon was recorded from with a microelectrode (microelectrode

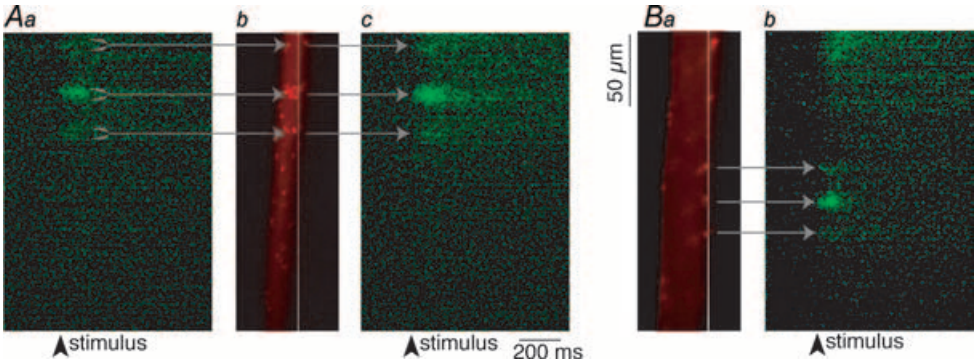

Figure 2. Sites of action potential-evoked Ca^{2+} entry and phalloidin puncta are colocalized at the presynaptic terminal
Aa, action-potential-evoked Ca^{2+} responses recorded using Ca^{2+}-sensitive dye, Oregon Green 488 BAPTA-1. Evoked Ca^{2+} entry occurs at discrete and localized 'hotpots' along the length of the axon, as shown here. *Ab*, injection of fluorescently labelled phalloidin (Alexa Fluor 568 phalloidin) into this axon marks phalloidin puncta (red) only at the same locations as evoked Ca^{2+} responses ($n = 9$ puncta). Every identifiable phalloidin punctum, conversely, demonstrates a resolvable Ca^{2+} signal ($n = 18$ phalloidin puncta, in 8 axons), both at the same region as previously measured (shown in *Ac*) and at other regions of same axon as in *B*. *Ba*, phallodin puncta at other regions of axon also show action-potential-evoked Ca^{2+} hotspots, as seen in *Bb*.

contained 1 M KCl) in the presence of 100 μM FM2-10 perfused over the ventral-medial tracts of the spinal cord (see Fig. 1*A*). The axon was stimulated 2000 times (2 Hz, with 2 ms depolarizing current pulses through the recording microelectrode) to cause exocytosis and subsequent compensatory endocytosis to label synaptic vesicle clusters with FM2-10. During the dye-loading stimulus protocol, postsynaptic activity was blocked with the glutamate receptor antagonists CNQX and AP5 (5 and 100 μM, respectively). Following this labelling step, the electrode was removed from the axon and excess dye was removed with Advasep 7 (Kay *et al.* 1999) at 1 mM for 1 min. After removal of Advasep 7 from the superfusate, dye puncta were observed on the periphery of the axons (Fig. 3*A*). The same axon was then re-impaled and pressure-injected with fluorescently labelled phalloidin (Alexa Fluor 568 phalloidin) through the microelectrode. The phalloidin labelling accumulated around the synaptic vesicle clusters confirming the earlier observation that phalloidin-labelled structures surround synaptic release sites (Pieribone *et al.* 1995; Shupliakov *et al.* 2002). In a total of six preparations, 40 FM puncta were counted, and all colocalized with the phalloidin labelling (Fig. 3*B* and *C*). All vesicle clusters along the giant colocalized with phalloidin puncta, indicative of the active zone localization of synaptic vesicles and their surrounding actin bundles.

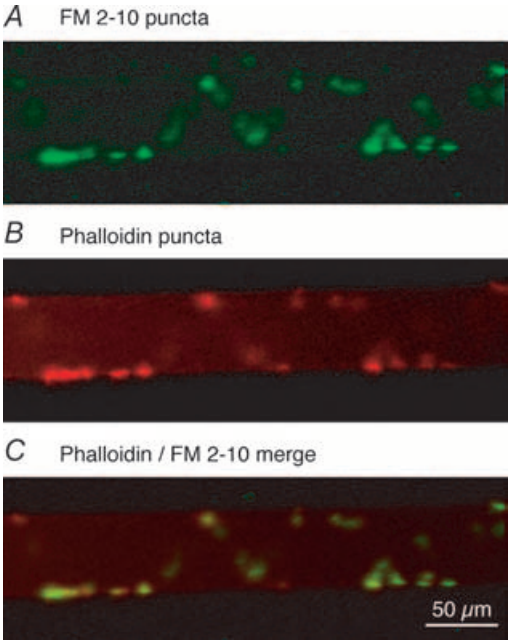

Figure 3. Recycling vesicle clusters colocalize with actin bundles at the presynaptic terminal
A giant axon was impaled with a microelectrode first containing KCl (1 M), and after FM staining with a second electrode containing labelled phalloidin (Alexa Fluor 568 phalloidin). FM 2-10 was applied to the ventral surface of the spinal cord as a continuous stream from a pipette (see Fig. 1*A*). *A*, FM2-10 was loaded into synaptic vesicles in lamprey giant axons by repetitive stimulation of a single axon through the KCl intracellular electrode in the presence of extracellular FM dye. On imaging the tissue, puncta of dye are observed along the periphery of the recorded axon. *B*, following the FM loading step, the same axon was re-impaled with a phalloidin-containing electrode. Presynaptic injection of fluorescent phalloidin into the same axon reveals location of actin clusters surrounding vesicles. *C*, overlay of *A* and *B* demonstrates that the location and structure of the phalloidin-labelled actin bundles (*B*) show an identical distribution to the vesicle clusters (*A*). In a total of 5 preparations, all observable puncta ($n = 40$) showed colocalization.

The effect of phalloidin on synaptic transmission

Phalloidin colocalizes with the presynaptic terminal. Previous studies in the lamprey giant synapse have demonstrated that phalloidin labelling surrounds presynaptic structures within the giant axon and that actin may play a role in vesicle recycling (Shupliakov *et al.* 2002), although this hypothesis has been challenged (Sankaranarayanan *et al.* 2003). Using simultaneous paired recordings of presynaptic giant reticulospinal axons and their postsynaptic partners we investigated the effect of phalloidin treatment on synaptic efficacy. Paired-cell recordings were made as in Fig. 1. Phalloidin was pressure injected into the presynaptic terminal, and the targeting of phalloidin to presynaptic actin was monitored by measuring the fluorescence intensity of puncta labelled by the phalloidin (Fig. 4*A* (green) and *D*). Immediately following phalloidin injection and after the formation of distinct presynaptic fluorescent puncta, synaptic transmission was unaffected. However, over a period varying from 5 min to over 10 min recorded in five such paired-cell recordings stimulated at 15 s intervals, synaptic transmission was blocked (Fig. 4*B* and *C*; τ of exponential decay fitted to EPSC amplitude $= 2.5 \pm 0.8$ min). Over this period no further increase in phalloidin fluorescence was observed (Fig. 4*D*). At these giant synapses, we have previously determined that the readily releasable pool of primed vesicles – those whose release is not blocked by botulinum toxins – requires between 200 and 400 stimuli for depletion. Additionally, without high-frequency stimulation, this pool of vesicles remains functional for in excess of 20 min (Gerachshenko *et al.* 2005). It is apparent that phalloidin inhibits synaptic transmission more rapidly than is necessary for recycling of vesicles, and more rapidly than could be accounted for by loss of the primed pool and its replacement by any putative actin-dependent mechanism.

Characterization of action-potential-evoked Ca^{2+} transients

We have demonstrated that FM-dye-labelled vesicles, actin clusters and physiologically evoked localized Ca^{2+}

entry colocalize at the same sites. Ca^{2+}, whether immediately effecting release by achieving micromolar or greater concentrations in the presynaptic specialization, or by modulating release at lower concentrations, has a profound impact on synaptic transmission. The presence of Ca^{2+} channels or of a recordable Ca^{2+} transient at a particular location does not, however, indicate the reliability of the Ca^{2+} response when recorded over time.

To further characterize the spatial localization and dynamic properties of the action-potential-evoked Ca^{2+} transients, we performed Ca^{2+} imaging experiments directly on presynaptic terminals. Presynaptic axons were retrogradely labelled with Oregon Green 488 BAPTA-1, and single stimuli were applied to the spinal cord to evoke action potentials in the spinal cord. For these experiments, the ventral-medial tracts were stimulated with a tungsten microelectrode and the Ca^{2+} transient recorded over sequential stimuli. Using confocal microscopy, a single line along the edge of an axon was repetitively scanned at 2 ms intervals. Using this method, we could monitor the action-potential-evoked changes in presynaptic Ca^{2+} concentration with high spatial and temporal resolution. A single action potential evoked readily recordable Ca^{2+} transients in individual axons (Fig. 5). This Ca^{2+} response to action potential stimulation is stereotypical and reproducible. At each identified hotspot, repeated stimulation led to a response with similar peak amplitude and similar kinetics (Fig. 5*A* and *B*). Furthermore, the pattern of activation of hotspots and their locations on the surface of the axon were repeated accurately with each stimulus. In four axons, the mean peak amplitudes of action-potential-evoked Ca^{2+} transients were measured for at least three consecutive responses and the coefficient of variance (CV) of these responses was calculated (mean $CV = 0.027 \pm 0.008$). This measured variance of the response did not differ significantly from the variance calculated from the recording noise. This is very small compared with variance of the subsequent evoked synaptic response (mean CV of chemical EPSCs $= 0.5 \pm 0.2$, e.g. Fig. 1*C*).

Using the repeatability of the Ca^{2+} transient, it was possible to construct a two-dimensional image to describe the action-potential-evoked spread of Ca^{2+} within the axon. Axons were labelled as described, and single stimuli were applied extracellularly with a tungsten

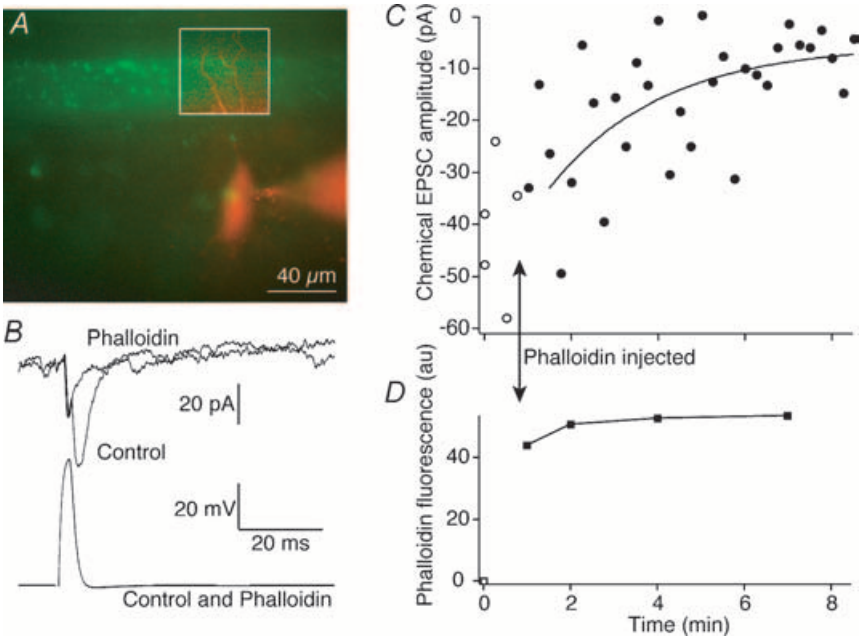

Figure 4. Phalloidin inhibits synaptic transmission
A, a merged image of presynaptic phalloidin (green) and postsynaptic Alexa 568 (red) showing the region of close apposition between the presynaptic axon and postsynaptic neurone during a paired recording. This region is outlined in the inset box where the contrast of the postsynaptic image was enhanced for clarity. *B*, postsynaptic responses (EPSCs; top) and presynaptic action potential (bottom) that evoked the EPSCs in the pair shown in the image in *A*. The responses are shown before (Control) and 8 min after presynaptic injection of phalloidin. Responses are the means of 4 sequential action potentials and EPSCs. *C*, time course of block of EPSCs (○, control responses; ●, after injection of phalloidin). The smooth curve is an exponential fit to the decay of the response ($\tau = 3.5$ min). *D*, time course of intensity of fluorescence of phalloidin puncta in the boxed region of *A*. Time course coincident with the electrophysiological data shown in *C*.

microelectrode. Stimuli were repeated approximately every 30 s. During stimuli, line scans were made over the same axon at the plasma membrane and at sequential increments inside the axon. An example is shown in Fig. 6. All of the line scans were performed in the same image focal plane shown as a single semi-transparent optical section through a three-dimensionally reconstructed axon (Fig. 6*A*). A plot of the line scan taken at the plasma membrane is shown (Fig. 6*B* and *C*), and the data extracted from the hotspot outlined in red are shown in red (Fig. 6*D*) as the largest and fastest peak. Results taken from the same hotspots, but measured at successive depths inside the axon, are shown as a series of nested curves in this plot. From this data, it was possible to generate a movie sequence of two-dimensional data to demonstrate the time course of entry, diffusion and sequestration of Ca^{2+} during and immediately after the action potential. This movie is shown as a sequence of eight frames representing the area of the axon outlined in a red rectangle in Fig. 6*B* (Fig. 6*F*). From this data, it is apparent that the time course of Ca^{2+} entry is very rapid, about 6 ms, which is within the depolarized phase of the action potential and the activation of the postsynaptic response to the release of neurotransmitter. In contrast, Ca^{2+} transients recorded at locations away from the synaptic zone and evoked Ca^{2+} hotspot showed a much slower response, rising to similar amplitudes as the late phase of the Ca^{2+} response recorded at the hotspot (Fig. 6*E*).

It was apparent from the imaging (Fig. 6*D* and *E*) that stimulus-evoked Ca^{2+} transients recorded at the giant axon plasma membrane achieved short-lived concentration spikes that decayed rapidly. After this short lifetime Ca^{2+} response, a longer-lived Ca^{2+} response was seen at all locations in the axon. We have analysed the relationship between these components of the Ca^{2+} response more fully.

The Ca^{2+} response at the centre of the hotspots was rapid: it was within the time course of the synaptic response and rose from baseline to peak within 6 ms. In Fig. 7*A* the time course of the Ca^{2+} response is compared with a typical synaptic response recorded separately from a paired cell recording in which a presynaptic action potential (Fig. 7*Ab*) evoked a postsynaptic EPSC (Fig. 7*Ac*). The Ca^{2+} response (4 pixels from the centre of the hotspot in Fig. 6) is shown to the same time scale as the action potential and EPSC (Fig. 7*Aa*), with the red vertical lines

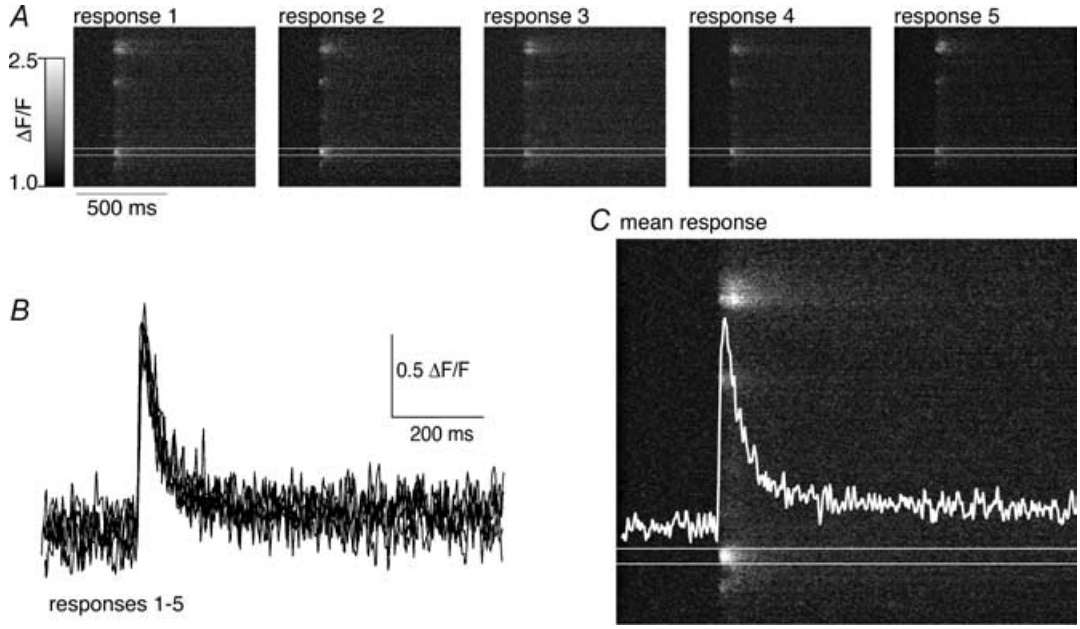

Figure 5. The spatial distribution and dynamic properties of Ca^{2+} transients are reproducible over repeated stimuli

A, an axon was retrogradely labelled with Ca^{2+}-sensitive dye (Oregon Green 488 BAPTA-1 dextran). The confocal laser line was scanned for 512 times over the same location at the plasma membrane surface of the axon (see Figs 2, and 6*A* and *B* for details) at 500 Hz. The resultant image is a plot of distance along the axon surface in the vertical plane and time in the horizontal axis. A single action potential is evoked leading to a punctate or 'hotspot' distribution of Ca^{2+} entry to the cytosol from along the axon surface. Five sequential responses to single action potentials are displayed. *B*, integrated plots of the rise in fluorescence taken from the 'hotspot' between the white lines in *A*. The graph is an overlay of all 5 responses demonstrating that the amplitude and rise and decay kinetics of the response is reproducible. *C*, the image is the mean of the images in *A*. The overlayed white trace is the mean of the traces in *B*.

indicating sample times of the imaged data. Because these data were not recorded at the same time, the uncertainty in the relative timing of the imaging data is indicated by the grey outline of the Ca^{2+} response. After subtraction of the electrical component of the postsynaptic EPSC (grey line Fig. 7*Ac*) the evoked chemical EPSC duration is revealed (black line) and this is clearly preceded by the Ca^{2+} signal recorded at the hotspot. In contrast, the Ca^{2+} signal recorded at the axon plasma membrane between hotspots shows a significant delay to initiation and a significantly slower rise time (Fig. 7*Ad*). These data indicate that the Ca^{2+} transient recorded between hotspots does not originate from voltage-activated Ca^{2+} channel opening generalized to any point on the axon surface. It

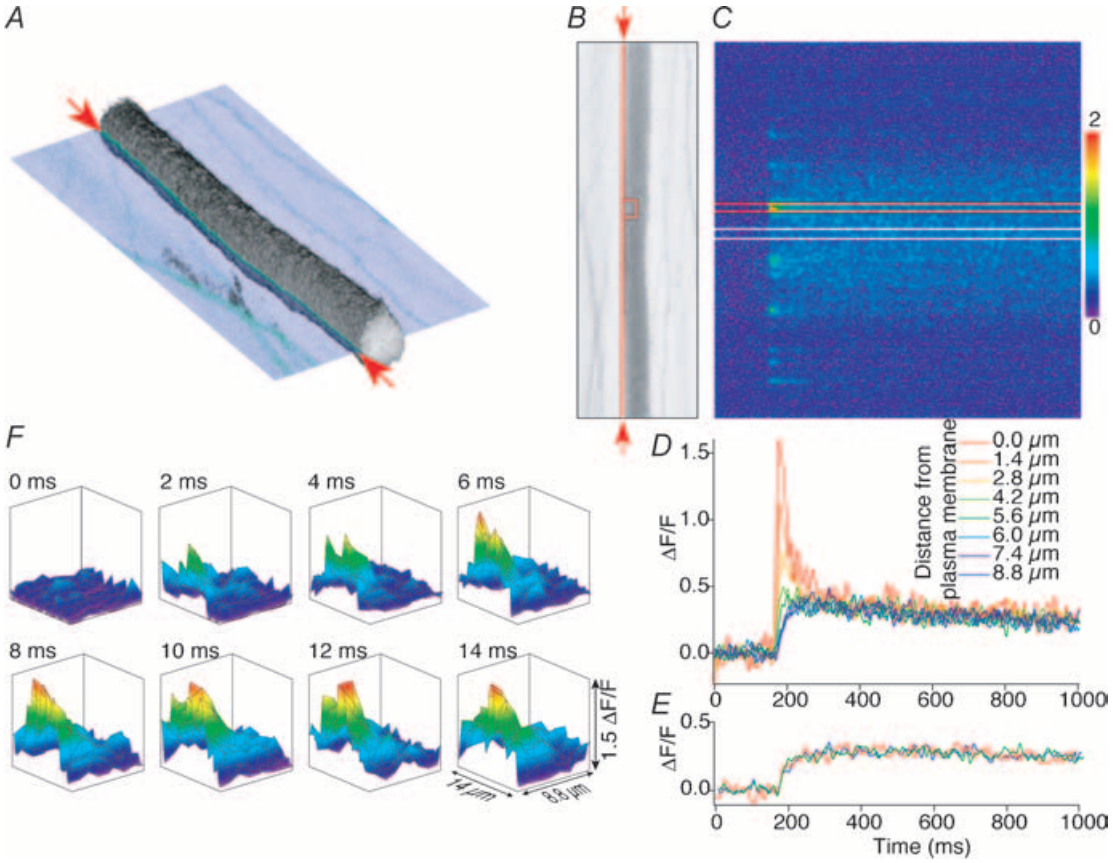

Figure 6. Characterization of action potential-evoked Ca^{2+} transients in reticulospinal axons
A, three-dimensional reconstruction of an axon labelled with Oregon Green dextran. The image is reconstructed from 60 sequential optical sections in the live intact spinal cord. Physiological data in the remainder of the figure is taken from line scans at the plane shown cutting through the three-dimensional image. The red arrows indicate the orientation and position of the line scanning performed across the plasma membrane. *B*, single optical section shown in *A* orientated orthogonally to the direction of view. The vertical red line between the red arrows indicates the location of the line scanned repeatedly and shown in *C*. *C*, line scan of the axon shown in *A* and *B* along the line indicated by the arrows at 500 Hz. The laser was scanned repetitively over the same line and the resultant fluorescence trace displayed with time along the *x*-axis against distance along the axon on the *y*-axis. A single stimulus was given (arrowhead), leading to transient increase in fluorescence level (i.e. $[Ca^{2+}]_i$). The colour scale refers to $\Delta F/F$. *D*, at discrete points at the plasma membrane (hotspots) the Ca^{2+} signal rises and decays rapidly. An integrated plot of a line scan from the part of *C* between the two red lines; the response recorded at the plasma membrane shown in *C* is the largest response in red. The smaller slower responses were obtained from line scans positioned sequentially 1.4 μm into the interior of the axon in the order indicated by the colour coding. *E*, between hotspots, the action-potential-evoked Ca^{2+} transients rise more slowly. An integrated plot of line scan from the part of *C* between the two white lines; the response recorded at the plasma membrane shown in *C* is the same as the response recorded 5.6 and 8.8 μm into the axon interior. *F*, the data from each line scan summarized for the integrated plots in *D* were replotted to represent an artificially constructed two-dimensional image of the Ca^{2+} transient. The colour-coded surface projections each form sequential virtual images of the Ca^{2+} transients at 2 ms intervals from the red rectangle over the axon in *B*.

must occur following a slower process or by diffusion to that location.

To determine whether diffusion from hotspots can account for the diffuse, slowly rising, Ca^{2+} signal, we performed a further analysis of the Ca^{2+} data presented as two-dimensional movie frames in Fig. 6. The Ca^{2+} transient fluorescent spikes in each of these frames was well fitted with a two-dimensional Gaussian fit (Fig. 7*B*). In each case, the sole constraint to the fitting function was to centre point (y_0) of the Gaussian perpendicular to the plane of the axon edge. This was centred at the plasma membrane as $y_0 = 0$. It was immediately apparent that the Ca^{2+} signal initiated at a point, and then expanded from that point as the fit curves extended along the axon edge and into the axon interior with each successive frame. The depth and width of these curves were analysed further in Fig. 7*C* to demonstrate that the width of the Ca^{2+} signal expanded equally rapidly into the axon and along the edge of the axon (data from fits of four hotspots from axons recorded in two preparations). These data are consistent with Ca^{2+} originating from a source at the site of the Ca^{2+} hotspot during and immediately after the depolarizing

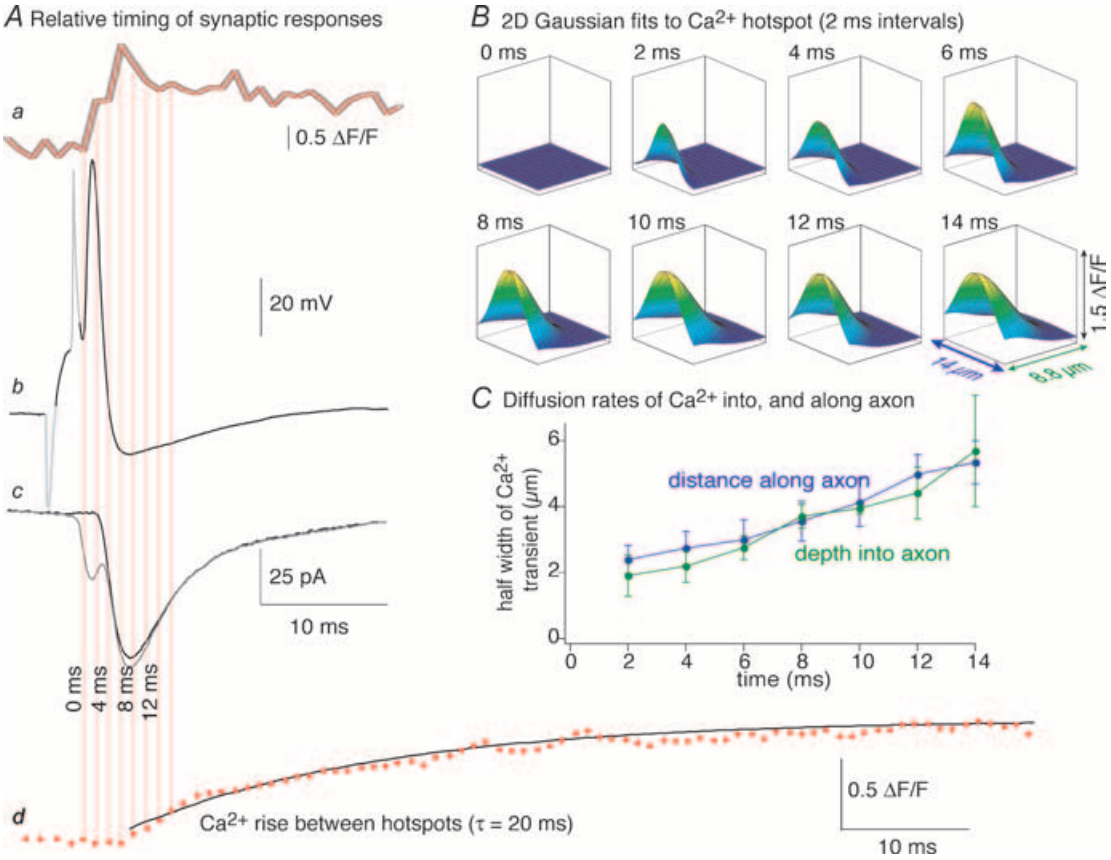

Figure 7. The relative timing of axon Ca^{2+} transients and the synaptic response
A, Ca^{2+} transients at hotspots in the presynaptic axon can account for synaptic release. *Aa*, Ca^{2+} transient measured from 4 pixels (1.4 μm), 0 μm from the axon membrane at the hotspot shown in Fig. 5. The grey outline represents the timing uncertainty with respect to the separately recorded synaptic pair in *Ab* and *Ac*. *Ab*, typical action potential evoked with a depolarizing pulse in a reticulospinal axon during paired-cell recording. Sections in grey represent the electrode capacitance transients (dimmed for clarity). *Ac*, postsynaptic response evoked in this cell recorded as a pair to the action potential in *Ab*. The grey trace is the average of 10 sequentially evoked synaptic responses. The black trace is the isolated chemical component after subtraction of the electrical component. *Ad*, Ca^{2+} transient recorded midway between hotspots (the region between the white lines in Fig. 5*C* and *E*). The time base is the same as for *Aa*–*Ac* (the *y*-axis is enlarged for clarity). The black curve is a single exponential fit to the rise of this transient. *B*, two-dimensional Gaussian fits to the data shown as surface plots in Fig. 5*F*. These represent an estimate of the spread of the Ca^{2+} transient at 2 ms intervals. *C*, four hotspots were analysed from two axons as in *B* above. The half-widths of the Gaussian fits were plotted with time for 7 frames following the stimulus. Note that the rate of spread of the transient is the same into the interior of the axon as it is along the plane of the axon plasma membrane.

phase of the action potential. Ca^{2+} is likely to reach the remainder of the interior of the axon following diffusion from these points of origin. Indeed the data taken 10 μm from the nearest visible hotspot (Fig. 7*Ad*) indicate that the Ca^{2+} transient takes approximately 30 ms to reach a half-maximum value, and 150 ms to peak, by which time the response is of uniform amplitude throughout the axon.

Ca^{2+} channels are not distributed widely on the axon membranes

While Ca^{2+} channels are localized to release zones, other ion channels may be more or less diffusely localized in the presynaptic membrane. Our imaging data support the hypothesis that Ca^{2+} transients mediated by single action potentials are initiated by localized sources on the axon plasma membrane restricted to synaptic zones.

Fluorescent Ca^{2+} transients were blocked entirely by Cd^{2+} (100 μM; data not shown), but more potently by Ni^{2+}. Ca^{2+} transients were again evoked by single stimuli applied to axons retrogradely labelled with Oregon Green BAPTA-1 dextran (Fig. 8*A*). This response was blocked in a dose-dependent manner by Ni^{2+} (Fig. 8*Ab* and *c*, and 8*C*; half-maximal inhibition at 2 μM Ni^{2+}; $n = 4$). Using patch electrodes containing Cs^{+} as the primary charge carrier in the patch solution and external solution containing Ba^{2+} (2.6 mM), TTX (1 μM) and 4-AP (1 mM), we recorded whole-cell Ba^{2+} currents in reticulospinal axons. Axons were voltage clamped at −80 mV, and 10 mV increments of test potential were applied from −80 to +40 mV to evoke a Ba^{2+} current. The peak current was measured at each test potential to generate a current–voltage plot (Fig. 8*B*). Similar to the imaged Ca^{2+} transient, this Ba^{2+} current was entirely blocked by Ni^{2+} (Fig. 8*B*), with a dose–response curve remarkably similar to the imaged Ca^{2+} transient

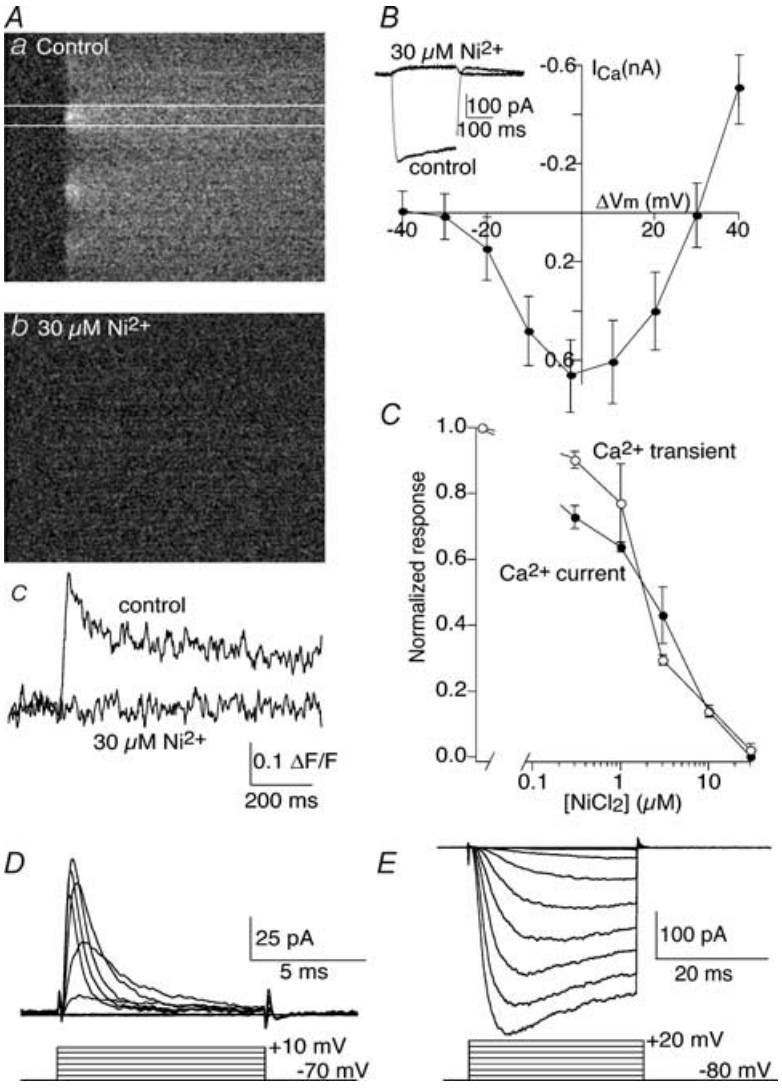

Figure 8. Ca^{2+} channels recorded with imaging and whole-cell patch recording are the same and are localized discretely on the axons
A, Ca^{2+} transients recorded by imaging are blocked by Ni^{2+}. *Aa*, line-scan image of an axonal Ca^{2+} response to a single action potential. Ca^{2+} transients imaged in this manner are localized to discreet regions on the axons. *Ab*, application of 30 μM Ni^{2+} abolishes these transients. *Ac*, the data between the white lines in *a* and *b* are replotted as a graph. *B*, whole-cell Ba^{2+} currents are high-voltage activated and blocked by Ni^{2+}. The inset shows an example of a whole-cell Ba^{2+} current activated by depolarizing voltage step from −80 to 0 mV. Application of Ni^{2+} (30 μM) abolished this current. The graph shows the peak current recorded from a sequence of such current steps from −80 to +40 mV averaged from 10 axons. *C*, superimposed dose–response curves of the effect of Ni^{2+} on imaged Ca^{2+} transients ($n = 4$), and of whole-cell Ba^{2+} currents ($n = 5$). The curves demonstrate a very similar half-maximal inhibition of the responses by Ni^{2+} (2.5 and 2.0 μM, respectively). *D*, Na^{+} currents are readily recorded by cell attached recording of the axons. The electrode contained Ringer solution and 4-aminopyridine (4-AP) (1 mM; $n = 5$). *E*, similarly, K^{+} currents are readily recorded in cell-attached configuration. The electrode contained Ringer solution and TTX (1 μM; $n = 6$).

(Fig. 8*C*; half-maximal inhibition at 2.5 μM Ni^{2+}; $n = 9$).

Macroscopic Ba^{2+} currents were reliably recorded from axons, but it was not possible to make cell-attached recordings of the same channels. In total, 150 cell-attached recordings were made from the surface of giant axons with electrodes containing 4-AP (1 mM), TTX (1 μM) and Ba^{2+} (100 mM). No depolarization-evoked currents were observed. Consequently, we hypothesize that the whole-cell Ba^{2+} current underlies the localized imaged Ca^{2+} transients.

In contrast, under cell-attached conditions, macroscopic Na^+ and K^+ currents were readily recorded from axons (Fig. 8*D* and *E*). Cell-attached recordings were made with electrodes containing Ringer solution to which either 4-AP (1 mM) or TTX (1 μM) was added to record voltage-activated Na^+ or K^+ currents, respectively. In all cases, the pipette was maintained at a holding potential of −80 mV and stepped from −70 through to +30 mV. In electrodes containing 4-AP, a rapidly activating and inactivating inward current was always recorded ($n = 4$); in electrodes containing TTX, a slower activating and non-inactivating outward current was always recorded ($n = 8$). The inward current's sensitivity to TTX and kinetics were entirely consistent with voltage-gated Na^+ channel activation; the outward conductance's sensitivity to 4-AP and kinetics were consistent with K^+ channel activation. We conclude that Ca^{2+} channels are clustered at active zones, while other (Na^+ and K^+) voltage-gated ion channels may be more diffusely located.

Comparison of action-potential-evoked Ca^{2+} transients with dyes of different affinities

The affinity of the Ca^{2+} dye Oregon Green 488 BAPTA-1 dextran to Ca^{2+} was obtained from standard buffered Ca^{2+} solutions (Molecular Probes) to which dye was added, and Ca^{2+} concentration–fluorescence curves were measured at physiological temperature (10°C). The affinity obtained in this way was somewhat lower than published data from the supplier and previous measurements from our laboratory at room temperature (566 nM at 10°C, this value varies considerably with temperature) and a sixfold increase in fluorescence between 0 μM Ca^{2+} bound to a saturating concentration of 40 μM ($F_{max}/F_{min} = 6$) was observed. We calculated resting Ca^{2+} levels from axons retrogradely labelled with Fura dextran as 100 nM ($n = 3$; not shown) Using this resting Ca^{2+} concentration, the k_D of Oregon Green 488 BAPTA-1 dextran at 10°C, and the fluorescence measured in control conditions and evoked by stimuli, estimates were made of the evoked Ca^{2+} transient concentrations using the following equation.

$$[Ca^{2+}] = k_d \frac{(F - F_{min})}{(F_{max} - F)}$$

Given the ratios of $F_{max}/F_{min} = 6$, and $F_r/F_{min} = 1.8$ (calculated from data with Fura dextran, assuming Oregon Green shows a k_D of 566 nM and resting Ca^{2+} is 100 nM), and the calibration curve obtained for Oregon Green 488 BAPTA-1 dextran, we can calculate $[Ca^{2+}]$ (nM) during the action potential evoked response.

$$566\frac{(1.8(F_t/F_r)F_{min} - F_{min})}{(6F_{min} - 1.8(F_t/F_r)F_{min})}$$

Where F_t/F_r is the ratio of transient fluorescence (F_t) to resting fluorescence (F_r). At the peak of the transient $F_t/F_r = 2.6$. This gives a Ca^{2+} transient peak concentration of 1.6 μM. In contrast the peak of the plateau concentration shows a ratio $F_t/F_r = 1.4$, which indicates a concentration of approximately 250 nM.

In order to obtain a second estimate of the Ca^{2+} response, we used a dye of lower affinity to quantify the amplitudes of these Ca^{2+} transients. Confocal microscopy was performed as described above, only this time axons were retrogradely labelled with Fluo-4 dextran ($k_D = 28$ μM at 10°C, $F_{max}/F_{min} = 40$). Measurement of the single-action-potential-evoked Ca^{2+} transients with Fluo-4 dextran revealed a similar qualitative distribution of hotspots at the axonal membrane. A comparison of the response to a single shock measured with OGB1 and Fluo-4 is shown in Fig. 9. The rise times of the responses are similar and are essentially at the limit of detection using the line-scan acquisition method. The Ca^{2+} transients measured using the high-affinity dye Oregon Green BAPTA-1 dextran showed two phases of decay, a fast decay with a τ of 34 ± 2 ms and a slow decay of a smaller component with a τ of 1200 ± 100 ms (Fig. 9*B*; $n = 5$). The slow component was identical in amplitude to responses recorded away from hotspots. The low-affinity dye Fluo-4 dextran revealed the early decay phase only ($\tau = 44 \pm 5$ ms, $n = 3$) with no later plateau phase. Although the responses have similar amplitude, this does not automatically indicate that similar Ca^{2+} concentrations were detected in the two experiments. Because the experiments were performed in two different preparations, the results were scaled to illustrate the rapid rise time of the evoked Ca^{2+} response and the qualitative difference in the ability of the dyes to record the peak and residual components of the Ca^{2+} transients. Using the same equations to calculate the recorded Ca^{2+} concentration at the peak of the Ca^{2+} transient, but with data obtained from calibration curves for Fluo-4 dextran at 10°C (k_D of Fluo-4 dextran is 28 μM, and F_{max}/F_{min} is 40), revealed a Ca^{2+} transient with a peak amplitude of approximately 1.5 μM (a maximum of threefold increase in fluorescence on stimulation). This latter amplitude is at the very low range of the sensitivity of the dye, but is not far from agreement with the result using Oregon Green 488 BAPTA-1 dextran (1.6 μM). It is important to note, however, that although we may estimate the

presynatic Ca^{2+} concentration achieved at the synapse, this undoubtedly underestimates the Ca^{2+} concentration necessary to evoke release. Rather our estimate is likely to represent a minimum concentration that must be exceeded to evoke release. This is because the diffusional distance for Ca^{2+} signalling between the channel and its target machinery is less than the resolution of any light microscopic technique. Our imaging necessarily averages Ca^{2+} concentrations over a larger volume. In addition, the lack of plateau response using the low-affinity dye (Fluo-4 dextran) may at first seem anomalous, but results from two features of these dyes. The Oregon Green BAPTA-1 response was toward the peak of its dose–response curve over a response range that is not linear. Thus the recorded value of $\Delta F/F$ for the peak of the response was much smaller than a linear scaling of the plateau response. The peak of the response using the low-affinity Fluo-4 dextran, in contrast, was within the linear range of the response of the dye to Ca^{2+}. Thus even if the dye acted as a perfect Ca^{2+} reporter, the peak of the response would be much larger with respect to the plateau response than when recorded with Oregon Green BAPTA-1. However, the dye did not respond at all to very low Ca^{2+} concentrations within the resting Ca^{2+} concentration in the axon. It showed a linearity at very low Ca^{2+} concentrations that prevented recording Ca^{2+} signals in the 100 s of nanomolar range with this dye at this temperature. Indeed, the best fit of the Hill equation to calibration data for this dye indicates a Hill coefficient slightly greater than unity, which also indicates caution when using Ca^{2+}-sensitive dyes to measure absolute Ca^{2+} concentrations.

Single-action-potential-evoked Ca^{2+} transients are not affected by ryanodine

Ryanodine acts to unload internal Ca^{2+} stores by binding to RYR receptors (Bers & Fill, 1998), and has been shown at the lamprey reticulospinal synapse to modulate the Ca^{2+} transients in response to multiple action potentials (Cochilla & Alford, 1998). Our imaging data can be accounted for solely by Ca^{2+} entry through discretely localized voltage-gated Ca^{2+} channels. However, we wished to investigate the role, if any, of internal stores in modulation of Ca^{2+} transients evoked by single action potentials. Line-scan confocal microscopy was performed on axons retrogradely labelled with Oregon Green 488 BAPTA-1, and a single action potential was applied extracellularly. During stimuli, line scans were made over the axons at the plasma membrane. We measured the amplitude of responses at hotspots of Ca^{2+} entry along the length of the axon in control (Fig. 10*A*). After addition of ryanodine (20 μM) to the superfusate, we repeated the experiment and recorded evoked Ca^{2+} responses along the same edge of the axonal membrane as in control (Fig. 10*B*). Ryanodine had no significant effect on amplitude of the Ca^{2+} transients seen in response to single action potentials ($\Delta F/F$ in control $= 0.21 \pm 0.05$, $\Delta F/F$ in ryanodine $= 0.21 \pm 0.05$; $P < 0.05$; $n = 3$ preparations). We conclude that Ca^{2+} released from internal stores does not affect the responses recorded at hotspots in response to single action potentials.

Discussion

We have demonstrated the functional colocalization of known synaptic markers at the lamprey reticulospinal synapse. Our electrophysiological evidence and fluorimetric data suggest the active zone location of action-potential-driven Ca^{2+} transients, synaptic vesicle clusters and actin filaments known to surround vesicle clusters. Like Shupliakov *et al.* (2002) and Pieribone *et al.* (1995), we have shown that actin filaments surround vesicle clusters. In addition, we have validated the synaptic location of these actin filaments by demonstrating that they occur at sites of physiologically stimulated vesicle recycling, and that these vesicles and filaments

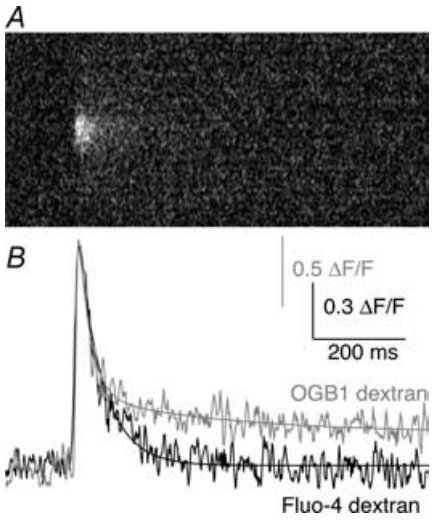

Figure 9. Comparison of evoked Ca^{2+} responses using Ca^{2+} –sensitive dyes of different affinities
Single-action-potential-evoked presynaptic Ca^{2+} transients were measured using Oregon Green 488 BAPTA-1 (OGB1; high affinity, k_D 566 nM at 10°C) and Fluo-4 dextran (low affinity, k_D 28 μM at 10°C). *A*, representative Ca^{2+} transient evoked by a single action potential recorded by Fluo-4 dextran. *B*, a comparison of the evoked responses measured with OGB1 and Fluo-4 dextran. The peak amplitudes are arbitrarily normalized to the same scale in this graph to emphasize the difference in kinetics of the decay rates. Because of its higher affinity, the OGB1 dextran can detect the late phase of the action-potential-evoked Ca^{2+} transient, and this response was best fit with two exponentials ($\tau = 25$ and 700 ms). In contrast, only the early (hotspot) phase of the response is recorded with Fluo-4 dextran because the late-phase transient does not reach a concentration that makes a significant change in Fluo-4 dextran fluorescence. This decay is best fit with a signal exponential ($\tau = 52$ ms).

colocalize with stimulated Ca^{2+} entry hotspots at these sites.

At lamprey presynaptic terminals, phalloidin puncta are observed to directly appose postsynaptic dendrites of motoneurones in the spinal cord. All phalloidin puncta in these axons colocalize with Ca^{2+} hotspots and conversely Ca^{2+} responses are seen at all points previously identified with phalloidin. In addition, synaptic vesicles marked with FM dyes also show colocalization with phalloidin puncta. Taken together, these results indicate the presence of three synaptic markers at release sites: synaptic vesicles, actin filaments and voltage-operated Ca^{2+} channels.

While actin is clearly present around synaptic vesicle clusters, it is less clear what role it plays in synaptic transmission. In this study we have used phalloidin, both as a marker of presynaptic terminals, and also as an inhibitor of actin depolymerization selectively applied to the presynaptic terminal. Phalloidin had no effect on Ca^{2+} entry to the presynaptic terminal, but it inhibited synaptic transmission over time courses shorter than can be explained by a simple exhaustion of the readily releasable pool (Gerachshenko *et al.* 2005; at least 200 stimuli were required to exhaust this pool after cleavage of synaptobrevin with botulinum toxin B injected directly into the presynaptic terminal). However, the role of actin in the synaptic vesicle cycle remains somewhat controversial. In the lamprey, it has previously been reported that phalloidin disrupts endocytosis and transport of recycled vesicles to the synaptic vesicle cluster at the presynaptic terminal (Shupliakov *et al.* 2002). Our data indicate stabilization of F-actin with phalloidin might also interfere with the recruitment of vesicles within or to releasable pools. In contrast at the calyx synapse of Held phalloidin has been reported to have little or no effect on release *per se*, although it may reverse the effects of the actin depolymerizing agent Latrunculin A (Sakaba & Neher, 2003), and actin is perhaps important in the transition of vesicles between reserve and readily releasable pools. Indeed, actin has been proposed to play a role in vesicle mobilization in other studies (Cole *et al.* 2000). In contrast, in hippocampal cultures, actin has been proposed to play an important role late in the fusion process (Morales *et al.* 2000). Consequently, while the role of actin in synaptic vesicle recycling remains controversial, it seems most likely that it plays an active role (Shupliakov *et al.* 2002) in this process, rather than a merely passive structural role (Sankaranarayanan *et al.* 2003). Actin may thus play numerous roles in the synaptic vesicle cycle and indeed while interactions of actin with synapsins clearly play a structural role in the reserve pool (Pieribone *et al.* 1995), these interactions may prove to be much more complex (Hilfiker *et al.* 2005).

There is evidence at other presynaptic terminals of Ca^{2+} channel clustering at active zones (Robitaille *et al.* 1990; Haydon *et al.* 1994; Kawasaki *et al.* 2004; Sidi *et al.* 2004; Wachman *et al.* 2004). In this study, we have presented evidence that substantially all of the action-potential-evoked Ca^{2+} entry to the axon occurs at these synaptic active zones. This conclusion is drawn from measurements of similar diffusion times into the core of the axon and along the axon perimeter, as well as the measurable delay seen between the initiation of the Ca^{2+} transients at synaptic hotpsots and the Ca^{2+} transient seen between these structures. In addition, no Ca^{2+} transients were recorded that did not subsequently prove to colocalize with other synaptic markers, and synaptic markers always predicted the presence of a stimulus-evoked Ca^{2+} transient. Variations in active zone size, measured with phalloidin, FM dye and Ca^{2+}-sensitive dye, were evident. This is likely to reflect known variability at these synapses that have been previously described as simple (with one active zone) or, more rarely, as

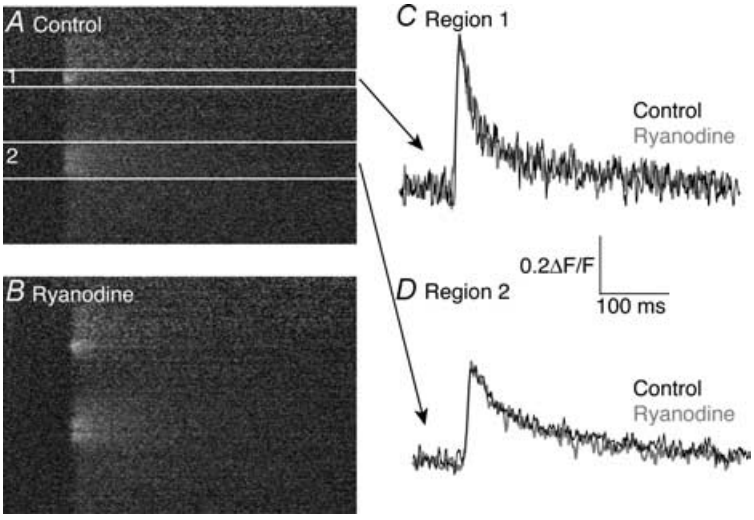

Figure 10. Ryanodine does not affect Ca^{2+} transients seen in response to single action potentials
Action-potential-evoked Ca^{2+} responses were measured in control (*A*) and in the presence of 20 μM ryanodine (*B*). Measurement of the amplitude of the Ca^{2+} response evoked by a single action potential at two discrete locations along the axon (regions 1 and 2) showed no significant difference between the control responses and those recorded in ryanodine (*C* and *D*).

complex with up to three active zones (Gustafsson *et al.* 2002).

Our ability to readily record Na^+ and K^+ conductances from axon membranes, but not Ca^{2+} currents, supports this conclusion. That we were readily able to record whole-cell Ca^{2+} currents but not cell-attached currents from the axon plasma membrane implies a structural localization of the Ca^{2+} channels underlying the whole-cell current. Failure to record the currents in cell-attached configurations may be because of simple probability, but might also result from the structure of the synapse. If axonal Ca^{2+} channels are at the presynaptic active zone, then all will be covered by a postsynaptic spine that may preclude their access to the recording electrode. A three-dimensonal view of these *en passant* synapses shows the presence of active zones directly apposed to (and presumably concealed by) dendritic arbors of postsynaptic cells. Consequently, we are able to record discrete and localized distribution of Ca^{2+} hotspots seen at the axonal plasmalemma with imaging methods, but do not have electrophysiological access to the clusters of Ca^{2+} channels at active zones.

Localized Ca^{2+} entry sites at presynaptic terminals have been demonstrated with Ca^{2+}-dependent luminescent proteins at the squid giant synapse (Llinas *et al.* 1995), with Ca^{2+} indicator dyes in frog (Issa & Hudspeth, 1996; DiGregorio & Vergara, 1997 DiGregorio *et al.* 1999; Wachman *et al.* 2004), bipolar cells (Zenisek *et al.* 2003) and at lamprey presynaptic terminals (Cochilla & Alford, 1998), although the relationship between these 'hotspots' and the associated presynaptic specializations has previously remained unclear except at ribbon synapses (Zenisek *et al.* 2004). We have now used fast line-scanning confocal microscopy to reliably image Ca^{2+} entry sites into lamprey giant axons, and have studied the spatial distribution of evoked Ca^{2+} transients responsible for release. We show with high temporal and spatial resolution, the time course and dynamic ranges of these Ca^{2+} responses. Action-potential-evoked Ca^{2+}entry into lamprey presynaptic terminals occurs at localized and discrete sites. These Ca^{2+} transients have a very rapid rise time (within 6 ms), their time course matches the depolarized phase of the action potential, they are unaffected by ryanodine, and they are blocked by blockers of Ca^{2+} channels (Cd^{2+} and Ni^{2+}, Takahashi *et al.* 2001). These physiological and functional characteristics of Ca^{2+} responses, taken together with their location at active zones, strongly support our hypothesis that the physiologically activated Ca^{2+} transients are recorded from Ca^{2+} channels at active zones and they correspond to anatomical correlates of presynaptic structures at active zones.

We have identified structural and functional components of neurotransmission at the lamprey reticulospinal synapse. Ca^{2+} channels responsible for release, synaptic vesicles and cytosketal elements are present at this synapse, in similar arrangements to those observed for other synapses. The relative locations of these ion channels, synaptic vesicles and cytoskeletal elements are important for the synchronicity, site-specificity and reliability of presynaptic terminal function.

References

Adler EM, Augustine GJ, Duffy SN & Charlton MP (1991). Alien intracellular calcium chelators attenuate neurotransmitter release at the squid giant synapse. *J Neurosci* **11**, 1496–1507.

Augustine GJ, Adler EM & Charlton MP (1991). The calcium signal for transmitter secretion from presynaptic nerve terminals. *Ann N Y Acad Sci* **635**, 365–381.

Bers DM & Fill M (1998). Coordinated feet and the dance of ryanodine receptors. *Science* **281**, 790–791.

Betz WJ & Bewick GS (1992). Optical analysis of synaptic vesicle recycling at the frog neuromuscular junction. *Science* **255**, 200–203.

Bloom O, Evergren E, Tomilin N, Kjaerulff O, Low P, Brodin L, Pieribone VA, Greengard P & Shupliakov O (2003). Colocalization of synapsin and actin during synaptic vesicle recycling. *J Cell Biol* **161**, 737–747.

Brodin L, Grillner S, Dubuc R, Ohta Y, Kasicki S & Hokfelt T (1988). Reticulospinal neurons in lamprey: transmitters, synaptic interactions and their role during locomotion. *Arch Ital Biol* **126**, 317–345.

Buchanan JT, Brodin L, Dale N & Grillner S (1987). Reticulospinal neurones activate excitatory amino acid receptors. *Brain Res* **408**, 321–325.

Catterall WA (1999). Interactions of presynaptic Ca^{2+} channels and snare proteins in neurotransmitter release. *Ann N Y Acad Sci* **868**, 144–159.

Cochilla AJ & Alford S (1998). Metabotropic glutamate receptor-mediated control of neurotransmitter release. *Neuron* **20**, 1007–1016.

Cochilla AJ & Alford S (1999). NMDA receptor-mediated control of presynaptic calcium and neurotransmitter release. *J Neurosci* **19**, 193–205.

Cole JC, Villa BRS & Wilkinson RS (2000). Disruption of actin impedes transmitter release in snake motor terminals. *J Physiol* **525**, 579–586.

Cooper RL, Winslow JL, Govind CK & Atwood HL (1996). Synaptic structural complexity as a factor enhancing probability of calcium-mediated transmitter release. *J Neurophysiol* **75**, 2451–2466.

DiGregorio DA, Peskoff A & Vergara JL (1999). Measurement of action potential-induced presynaptic calcium domains at a cultured neuromuscular junction. *J Neurosci* **19**, 7846–7859.

DiGregorio DA & Vergara JL (1997). Localized detection of action potential-induced presynaptic calcium transients at a *Xenopus* neuromuscular junction. *J Physiol* **505**, 585–592.

Dolphin AC (2003*a*). Beta subunits of voltage-gated calcium channels. *J Bioenerg Biomembr* **35**, 599–620.

Dolphin AC (2003*b*). G protein modulation of voltage-gated calcium channels. *Pharmacol Rev* **55**, 607–627.

Gerachshenko T, Blackmer T, Yoon EJ, Bartleson C, Hamm HE & Alford S (2005). Gbetagamma acts at the C terminus of SNAP-25 to mediate presynaptic inhibition. *Nat Neurosci* **8**, 597–605.

Gustafsson JS, Birinyi A, Crum J, Ellisman M, Brodin L & Shupliakov O (2002). Ultrastructural organization of lamprey reticulospinal synapses in three dimensions. *J Comp Neurol* **450**, 167–182.

Harlow ML, Ress D, Stoschek A, Marshall RM & McMahan UJ (2001). The architecture of active zone material at the frog's neuromuscular junction. *Nature* **409**, 479–484.

Haydon PG, Henderson E & Stanley EF (1994). Localization of individual calcium channels at the release face of a presynaptic nerve terminal. *Neuron* **13**, 1275–1280.

Heidelberger R, Heinemann C, Neher E & Matthews G (1994). Calcium dependence of the rate of exocytosis in a synaptic terminal. *Nature* **371**, 513–515.

Hell JW, Westenbroek RE, Elliott EM & Catterall WA (1994). Differential phosphorylation, localization, and function of distinct alpha 1 subunits of neuronal calcium channels. Two size forms for class B, C, and D alpha 1 subunits with different COOH-termini. *Ann N Y Acad Sci* **747**, 282–293.

Hilfiker S, Benfenati F, Doussau F, Nairn AC, Czernik AJ, Augustine GJ & Greengard P (2005). Structural domains involved in the regulation of transmitter release by synapsins. *J Neurosci* **25**, 2658–2669.

Ikeda SR (1996). Voltage-dependent modulation of N-type calcium channels by G-protein beta gamma subunits. *Nature* **380**, 255–258.

Issa NP & Hudspeth AJ (1996). The entry and clearance of Ca^{2+} at individual presynaptic active zones of hair cells from the bullfrog's sacculus. *Proc Natl Acad Sci U S A* **93**, 9527–9532.

Kawasaki F, Zou B, Xu X & Ordway RW (2004). Active zone localization of presynaptic calcium channels encoded by the cacophony locus of *Drosophila*. *J Neurosci* **24**, 282–285.

Kay AR, Alfonso A, Alford S, Cline HT, Holgado AM, Sakmann B, Snitsarev VA, Stricker TP, Takahashi M & Wu LG (1999). Imaging synaptic activity in intact brain and slices with FM1-43 in *C. elegans*, lamprey, and rat. *Neuron* **24**, 809–817.

Llinas R, Sugimori M & Silver RB (1992). Microdomains of high calcium concentration in a presynaptic terminal. *Science* **256**, 677–679.

Llinas R, Sugimori M & Silver RB (1995). Time resolved calcium microdomains and synaptic transmission. *J Physiol Paris* **89**, 77–81.

McClellan AD, McPherson D & O'Donovan MJ (1994). Combined retrograde labeling and calcium imaging in spinal cord and brainstem neurons of the lamprey. *Brain Res* **663**, 61–68.

Morales M, Colicos MA & Goda Y (2000). Actin-dependent regulation of neurotransmitter release at central synapses. *Neuron* **27**, 539–550.

Morgan JR, Di Paolo G, Werner H, Shchedrina VA, Pypaert M, Pieribone VA & De Camilli P (2004). A role for talin in presynaptic function. *J Cell Biol* **167**, 43–50.

Pieribone VA, Shupliakov O, Brodin L, Hilfiker-Rothenfluh S, Czernik AJ & Greengard P (1995). Distinct pools of synaptic vesicles in neurotransmitter release. *Nature* **375**, 493–497.

Richards MW, Butcher AJ & Dolphin AC (2004). Ca^{2+} channel beta-subunits: structural insights AID our understanding. *Trends Pharmacol Sci* **25**, 626–632.

Robitaille R, Adler EM & Charlton MP (1990). Strategic location of calcium channels at transmitter release sites of frog neuromuscular synapses. *Neuron* **5**, 773–779.

Rosenmund C, Rettig J & Brose N (2003). Molecular mechanisms of active zone function. *Curr Opin Neurobiol* **13**, 509–519.

Rovainen CM (1974). Synaptic interactions of reticulospinal neurons and nerve cells in the spinal cord of the sea lamprey. *J Comp Neurol* **154**, 207–223.

Sakaba T & Neher E (2003). Involvement of actin polymerization in vesicle recruitment at the calyx of held synapse. *J Neuroscience* **23**, 837–846.

Sankaranarayanan S, Atluri PP & Ryan TA (2003). Actin has a molecular scaffolding, not propulsive, role in presynaptic function. *Nat Neurosci* **6**, 127–135.

Schneggenburger R & Neher E (2000). Intracellular calcium dependence of transmitter release rates at a fast central synapse. *Nature* **406**, 889–893.

Shahrezaei V & Delaney KR (2004). Consequences of molecular-level Ca^{2+} channel and synaptic vesicle colocalization for the Ca^{2+} microdomain and neurotransmitter exocytosis: a monte carlo study. *Biophys J* **87**, 2352–2364.

Shupliakov O, Bloom O, Gustafsson JS, Kjaerulff O, Low P, Tomilin N, Pieribone VA, Greengard P & Brodin L (2002). Impaired recycling of synaptic vesicles after acute perturbation of the presynaptic actin cytoskeleton. *Proc Natl Acad Sci U S A* **99**, 14476–14481.

Shupliakov O, Low P, Grabs D, Gad H, Chen H, David C, Takei K, De Camilli P & Brodin L (1997). Synaptic vesicle endocytosis impaired by disruption of dynamin–SH3 domain interactions. *Science* **276**, 259–263.

Sidi S, Busch-Nentwich E, Friedrich R, Schoenberger U & Nicolson T (2004). gemini encodes a zebrafish L-type calcium channel that localizes at sensory hair cell ribbon synapses. *J Neurosci* **24**, 4213–4223.

Smith SJ, Buchanan J, Osses LR, Charlton MP & Augustine GJ (1993). The spatial distribution of calcium signals in squid presynaptic terminals. *J Physiol* **472**, 573–593.

Spafford JD & Zamponi GW (2003). Functional interactions between presynaptic calcium channels and the neurotransmitter release machinery. *Curr Opin Neurobiol* **13**, 308–314.

Takahashi M, Freed R, Blackmer T & Alford S (2001). Calcium influx-independent depression of transmitter release by 5-HT at lamprey spinal cord synapses. *J Physiol* **532**, 323–336.

Tareilus E & Breer H (1995). Presynaptic calcium channels: pharmacology and regulation. *Neurochem Int* **26**, 539–558.

Wachman ES, Poage RE, Stiles JR, Farkas DL & Meriney SD (2004). Spatial distribution of calcium entry evoked by single action potentials within the presynaptic active zone. *J Neurosci* **24**, 2877–2885.

Walrond JP & Reese TS (1985). Structure of axon terminals and active zones at synapses on lizard twitch and tonic muscle fibers. *J Neurosci* **5**, 1118–1131.

Zamponi GW (2001). Determinants of G protein inhibition of presynaptic calcium channels. *Cell Biochem Biophys* **34**, 79–94.

Zamponi GW (2003). Regulation of presynaptic calcium channels by synaptic proteins. *J Pharmacol Sci* **92**, 79–83.

Zenisek D, Davila V, Wan L & Almers W (2003). Imaging calcium entry sites and ribbon structures in two presynaptic cells. *J Neurosci* **23**, 2538–2548.

Zenisek D, Horst NK, Merrifield C, Sterling P & Matthews G (2004). Visualizing synaptic ribbons in the living cell. *J Neurosci* **24**, 9752–9759.

Zhai RG & Bellen HJ (2004). The architecture of the active zone in the presynaptic nerve terminal. *Physiology (Bethesda)* **19**, 262–270.

Zhang L, Volknandt W, Gundelfinger ED & Zimmermann H (2000). A comparison of synaptic protein localization in hippocampal mossy fiber terminals and neurosecretory endings of the neurohypophysis using the cryo-immunogold technique. *J Neurocytol* **29**, 19–30.

Acknowledgements

We would like to thank Eric Schwartz, Tatyana Gerachshenko and Roy Smetana for critical reading of the manuscipt. We also acknowledge Dr James Buchanan for many helpful comments. This work was supported by the NIMH grant number MH 64763.